CHEMISTRY OF MATERIALS

Article

pubs.acs.org/cm

Exceptional Gas Adsorption Properties by Nitrogen-Doped Porous Carbons Derived from Benzimidazole-Linked Polymers

Babak Ashourirad, Ali Kemal Sekizkardes, Suha Altarawneh,[†] and Hani M. El-Kaderi*

[†]Department of Chemistry, Virginia Commonwealth University, Richmond, Virginia 23284-2006, United States

Supporting Information

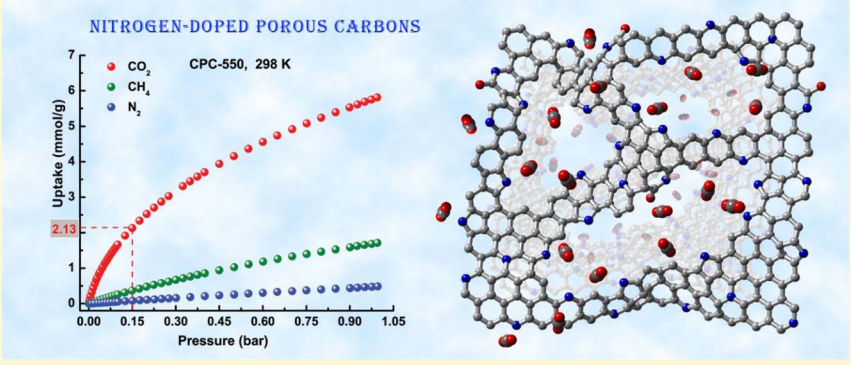

ABSTRACT: Heteroatom-doped porous carbons are emerging as platforms for use in a wide range of applications including catalysis, energy storage, and gas separation or storage, among others. The use of high activation temperatures and heteroatom multiple-source precursors remain great challenges, and this study aims to addresses both issues. A series of highly porous N-doped carbon (CPC) materials was successfully synthesized by chemical activation of benzimidazole-linked polymers (BILPs) followed by thermolysis under argon. The high temperature synthesized CPC-700 reaches surface area and pore volume as high as 3240 $m^2\ g^{-1}$ and 1.51 $cm^3\ g^{-1}$, respectively, while low temperature activated CPC-550 exhibits the highest ultramicropore volume of 0.35 $cm^3\ g^{-1}$. The controlled activation process endows CPCs with diverse textural properties, adjustable nitrogen content (1−8 wt %), and remarkable gas sorption properties. In particular, exceptionally high CO_2 uptake capacities of 5.8 mmol g^{-1} (1.0 bar) and 2.1 mmol g^{-1} (0.15 bar) at ambient temperature were obtained for materials prepared at 550 °C due to a combination of a high level of N-doping and ultramicroporosity. Furthermore, CPCs prepared at higher temperatures exhibit remarkable total uptake for CO_2 (25.7 mmol g^{-1} at 298 K and 30 bar) and CH_4 (20.5 mmol g^{-1} at 298 K and 65 bar) as a result of higher total micropores and small mesopores volume. Interestingly, the N sites within the imidazole rings of BILPs are intrinsically located in pyrrolic/pyridinic positions typically found in N-doped carbons. Therefore, the chemical and physical transformation of BILPs into CPCs is thermodynamically favored and saves significant amounts of energy that would otherwise be consumed during carbonization processes.

1. INTRODUCTION

The increasing concentration of anthropogenic carbon dioxide in the atmosphere in recent decades is believed to be the main cause of global warming and climate change.[1,2] Therefore, carbon dioxide (CO_2) capture and sequestration (CCS) is regarded as a short-term solution until fossil fuels are replaced by renewable clean energy sources. The conventional approach for CCS, absorption by aqueous amine solutions, suffers from serious drawbacks such as corrosion of equipment, solvent evaporation and toxicity, and most importantly substantial energy cost for regeneration.[3] For cyclic CCS from the postcombustion flue gas mixtures, physisorption of CO_2 is preferred because the moderate CO_2/adsorbent interaction facilitates regeneration of sorbent. To this end, a wide spectrum of porous adsorbents including zeolites,[4,5] metal organic frameworks (MOFs),[6,7] porous organic polymers (POPs),[8,9] functionalized porous silica,[10,11] and porous carbons[12−14] have been developed for use in the CCS. Among these, MOFs and porous carbons have attracted considerable attention. MOFs can exhibit high CO_2 adsorption capacity at both low and high pressures because of their tunable physical and chemical nature.[15,16] However, some MOFs are water sensitive and made of metal ions. As such, finding alternative adsorbents that are green (metal-free) and chemically robust like porous carbons is highly desirable for gas storage and separation applications.

Porous carbons exhibit multifaceted desirable features such as high thermal and chemical stability, tunable textural properties, lightweight and metal-free framework, and ease of regeneration, and most importantly they can be prepared from renewable sources.[17,18] In addition to these properties, the

Received: December 2, 2014
Revised: January 21, 2015

DOI: 10.1021/cm504435m
Chem. Mater. XXXX, XXX, XXX−XXX

Scheme 1. Synthesis of N-Doped Porous Carbons

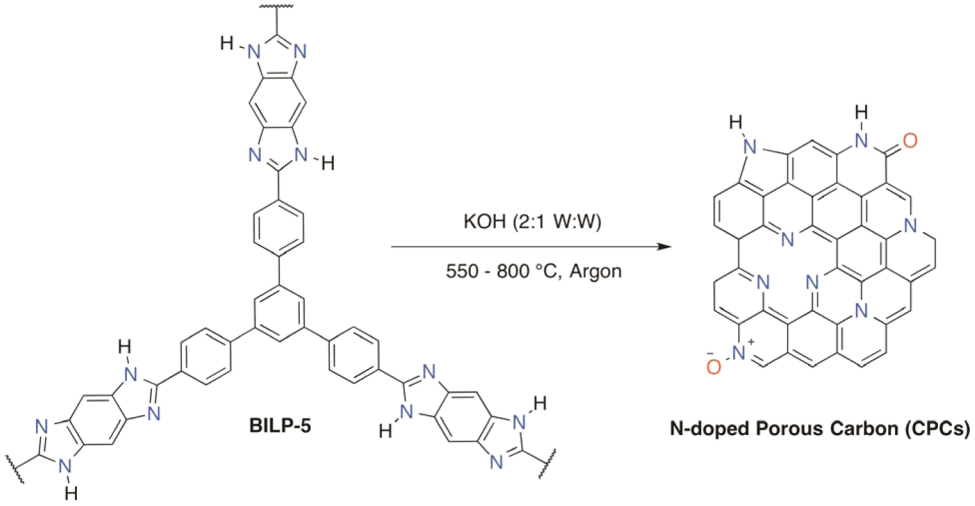

chemical and electronic nature of porous carbons can be tuned by integrating heteroatoms (i.e., N, B, P, S)[19] to access a wide range of applications including heterogeneous catalysis, energy storage, and gas storage and separation, among others. Unfortunately, commercially available porous carbons show moderate CO_2 capture capacity as well as low selectivity at ambient pressure.[20] Hence, recent efforts in this field have been directed toward porosity enhancement and chemical modification with heteroatoms to enhance CO_2 uptake and selective binding from gas mixtures. Modification methods include chemical and physical activation,[21−23] templated synthesis,[24−26] and impregnation with extra carbon framework (such as furfuryl alcohol).[27] In particular, activation and/or carbonization of porous architectures like MOFs or POPs led to highly functional nanoporous carbons.[27−32] Furthermore, incorporation of heteroatoms having Lewis basic properties has been suggested to simultaneously enhance CO_2 capture capacity and selectivity through Lewis acid−base interactions.[33−35] To prepare nitrogen doped porous carbons two main strategies have been developed: postsynthesis treatment of a carbonaceous precursor with ammonia and carbonization of nitrogen-rich carbon precursors such as biomass or organic polymers. The first approach is inefficient, is time-consuming, and usually demands high energy (in terms of heat). To fulfill the second approach on the other hand, a great deal of research has been devoted to the preparation of nitrogen doped carbons from biomass and nonporous synthetic polymers (such as polypyrrole, polyaniline, polyacrylonitrile).[36,37]

In this study, we demonstrate for the first time the use of porous and nitrogen-rich benzimidazole-linked polymers (BILPs) as single source precursors for the preparation of highly porous N-doped carbons (CPCs) that exhibit one of the highest CO_2 capture capacity and selectivity values reported to date for porous carbons. Controlled KOH activation of polymers led to a series of N-doped CPCs that feature variable N-content, porosity, and CO_2 capture properties as a function of thermolysis temperature. Notably, the N sites within the imidazole rings of BILPs are intrinsically located in pyrrolic/pyridinc positions typically found in N-doped carbons. Therefore, the chemical and physical transformations of BILPs into N-doped CPCs are thermodynamically favored and allow considerable reduction in energy consumption during carbonization stages.

2. EXPERIMENTAL SECTION

2.1. Materials and Methods. All starting materials and solvents were obtained from commercial sources and used without further purification, unless otherwise mentioned. KOH (99%) was purchased from Alfa Aesar. THF was dried by distillation over Na/benzophenone. BILP-5 was synthesized according to published methods.[33,34] Elemental microanalyses were performed at the Midwest Microlab, LLC. To obtain scanning electron microscopy (SEM) images, each sample was dispersed onto a sticky carbon surface attached to a flat aluminum sample holder. Then, the sample was coated with platinum at a pressure of 1×10^{-5} mbar in a nitrogen atmosphere for 90 s before imaging. SEM images were taken on a Hitachi SU-70 scanning electron microscope. TEM images were recorded on a JEOL 2010 apparatus operated at an accelerating voltage of 200 kV. Samples were dispersed in ethanol and then drop cast onto a 200 mesh carbon-coated copper grid. Powder X-ray diffraction data were collected on a Panalytical X'pert pro multi-purpose diffractometer (MPD). Samples were mounted on a sample holder and measured using Cu Kα. X-ray photoelectron spectroscopy (XPS) analysis was performed on a ThermoFisher ESCALAB 250 spectrometer employing an Al Kα (1486.68 eV) X-ray source equipped with a hemispherical analyzer. Atmospheric gas (N_2, CO_2, and CH_4) sorption measurements were carried out on a Quantachrome Autosorb iQ volumetric analyzer using UHP grade adsorbates. Prior to the adsorption analyses the samples were degassed at 200 °C for 12 h. The specific BET (Brunauer−Emmett−Teller) surface areas were calculated considering analysis requirements for microporous materials. BET assistant on Quantachrome V.3.0 software was used to correct the 0.05−0.30 classical range of P/P_0 and find the appropriate pressure range based on "consistency criteria" for microporous materials.[38,39] The specific surface area, pore volume, and pore size distribution (PSD) from the N_2 isotherms (77 K) were obtained by applying the quench solid density functional theory (QSDFT) on the adsorption branch and assuming slit-like geometry on carbon material kernel. Moreover, microporous textural properties were investigated using CO_2 adsorption isotherms (273 K) and applying nonlocal density functional theory (NLDFT) under similar assumptions. High pressure gas sorption measurements were performed using a VTI-HPVA-100 volumetric analyzer. High pressure total gas uptakes were calculated by reported literature methods and NIST Thermochemical Properties of Fluid Systems were applied for the calculations.[40−42]

2.2. Synthesis of CPCs. Samples of BILP-5 were dispersed and dried at 130 °C overnight in a static oven to increase the interfacial contact area with activation agent KOH. Activated BILP-5 precursors were thoroughly mixed with KOH in an agate with KOH/BILP-5 weight ratio of 2:1 after which the mixture was transferred to a tube

DOI: 10.1021/cm504435m
Chem. Mater. XXXX, XXX, XXX−XXX

furnace (MTF-wire wound single zone) for carbonization and activation. Simultaneous chemical activation and decomposition of nitrogen-rich polymer was carried out under a flow of Ar (99.9%) in a temperature range of 550 to 800 °C (heating rate: 3 °C/min and holding time: 3 h). After cooling to room temperature, the samples were thoroughly washed with 1.0 M HCl several times to remove any inorganic salts, followed by washing with 1.0 M NaOH to neutralize acid and then a large amount of distilled water until neutral pH was obtained. During acid and base treatment the carbons were soaked for at least 2 h to dissolve inorganic salts, metallic potassium, and other unreacted potassium compounds. The chemically activated porous carbons were denoted CPC-T, wherein T represents the activation temperature.

3. RESULTS AND DISCUSSION

3.1. Synthetic and Characterization Aspects. The synthesis route of CPCs is depicted in Scheme 1 while Figure 1 shows the SEM and TEM images of CPCs. As shown in SEM images 1A-C, all CPCs exhibit a network morphology composed of irregular particles (~300 nm). The degree of deviation from BILP-5 spherical morphology (Supporting Information Figure S1) is more pronounced at elevated activation temperatures. It has been reported that most of activated carbons lose their spherical morphology under harsh activation conditions (activator/precursor > 2).[43] However, maintaining spherical morphology under mild activation conditions or direct pyrolysis of spherical precursors is conceivable.[44−46] The TEM image of the high temperature activated sample, CPC-800, does not show any ordered domains consistent with its amorphous nature. The amorphous nature of CPCs was further supported by PXRD studies that revealed no diffraction peaks as shown in Supporting Information Figure S2. The nitrogen content of CPCs obtained by elemental analysis evidently decreases with respect to activation temperature (Table 1 and Supporting Information Table S1). Nevertheless, CPC-550 retains a considerable amount of nitrogen (~8 wt %) surpassing the nitrogen content of many recently reported N-doped porous carbon materials.[43,47−49]

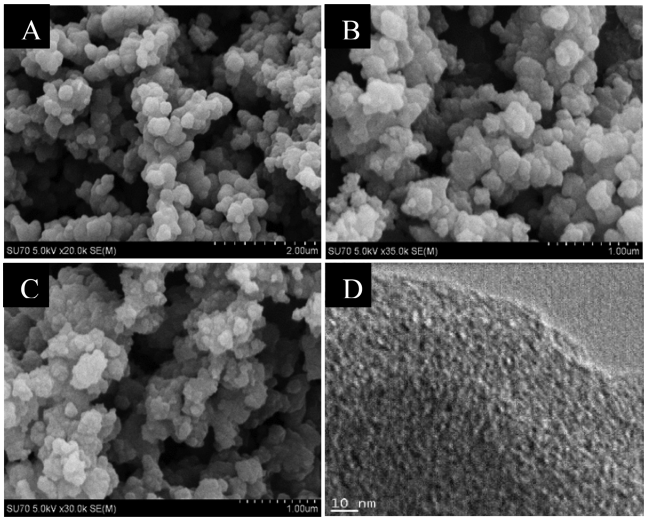

Figure 1. SEM images of CPC-600 (A), CPC-700 (B), and CPC-800 (C) and TEM image of CPC-800 (D).

3.2. Textural Properties. The specific surface area, pore volume, and pore size distribution of CPCs were comparatively characterized by means of nitrogen (77 K) and carbon dioxide (273 K) adsorption isotherms for micro-/mesopores and ultramicropores, respectively. The nitrogen sorption isotherms of all CPCs and BILP-5 are presented in Figure 2A and Supporting Information Figure S3. The isotherms of CPCs show a rapid nitrogen uptake at very low pressure region (P/P_0 < 0.01) followed by a plateau for most of the pressure range, suggesting that micropores are dominant in the samples. For all prepared carbons the knee between the very low pressure region and the flat plateau of nitrogen isotherms shifts to higher values as the activation temperature rises, which is likely due to narrow mesopores formation. The pore size distribution and cumulative pore volume of CPCs were probed by applying QSDFT and NLDFT on their N_2 (77 K) and CO_2 (273 K) isotherms, respectively. It is worth noting that the QSDFT model is superior for materials with surface chemical heterogeneity when nitrogen or argon are used to probe porosity.[50] Furthermore, the use of the CO_2 isotherm at 273 K proved to be very beneficial in analyzing subnanometer micropore distribution more accurately. In fact, the high kinetic energy of CO_2 at 273 K enables it to diffuse into narrower pores.[51] Pore size distributions are given in Figure 2B and Supporting Information Figure S5. For CPC-550, the PSD is mainly centered at 0.7 nm indicating the presence of dominant micropores. However, the appearance of a small peak at 2.2 nm for CPC-600 is related to the formation of narrow mesopores apart from pre-existing micropores. As the activation temperature increases, the mesopore peaks shift to higher values of 2.3 nm, 2.5 nm, and 3.1 nm for carbons activated at 650, 700, and 800 °C, respectively. Due to the highly microporous nature of prepared carbons, their subnanometer pore size distribution is also presented in Figure 2C and Supporting Information Figure S6. For most of the activated carbons, the fine micropores are distributed around 0.35 and 0.85 nm. Therefore, CPCs show a

Table 1. Textural Properties of BILP-5 and CPCs

sample	S_{BET}, [a] $m^2\ g^{-1}$	S_{Mic}, [b] $m^2\ g^{-1}$	V_{Mic}, [b] $cm^3\ g^{-1}$	V_{Tot}, [c] $cm^3\ g^{-1}$	$V_{Mic,DFT}$, [d] $cm^3\ g^{-1}$	$V_{Tot,DFT}$, [d] $cm^3\ g^{-1}$	V_0, [e] $cm^3\ g^{-1}$	D_{Pore}, [d] nm	yield %	N wt %	N/C molar
BILP-5	626	384	0.17	0.39	0.18 (55)	0.33	0.12	0.8	-	12.64	0.149
CPC-550	1630	1540	0.59	0.66	0.58 (97)	0.61	0.35	0.7	47	7.88	0.111
CPC-600	2059	1872	0.74	0.89	0.70 (88)	0.80	0.31	0.9	43	6.34	0.092
CPC-650	2967	2641	1.06	1.31	0.80 (67)	1.19	0.28	0.9/2.2	38	5.38	0.071
CPC-700	3242	2729	1.13	1.51	0.83 (61)	1.36	0.24	0.9/2.5	36	4.22	0.048
CPC-800	2872	1704	0.73	1.49	0.69 (51)	1.35	0.22	0.9/3.1	13	1.00	0.011

[a]Calculated in the partial pressure range which gives the best linear fitting. [b]Evaluated by the *t*-plot method. [c]Total pore volume at P/P_0 = 0.95. [d]Determined by cumulative pore volume and maxima of the PSD assuming slit-shaped pores and QSDFT model; the values in parentheses are the percentage of micropore volume relative to total pore volume. [e]Pore volume of ultramicropores (<0.7 nm) obtained from CO_2 adsorption data at 273 K.

DOI: 10.1021/cm504435m
Chem. Mater. XXXX, XXX, XXX−XXX

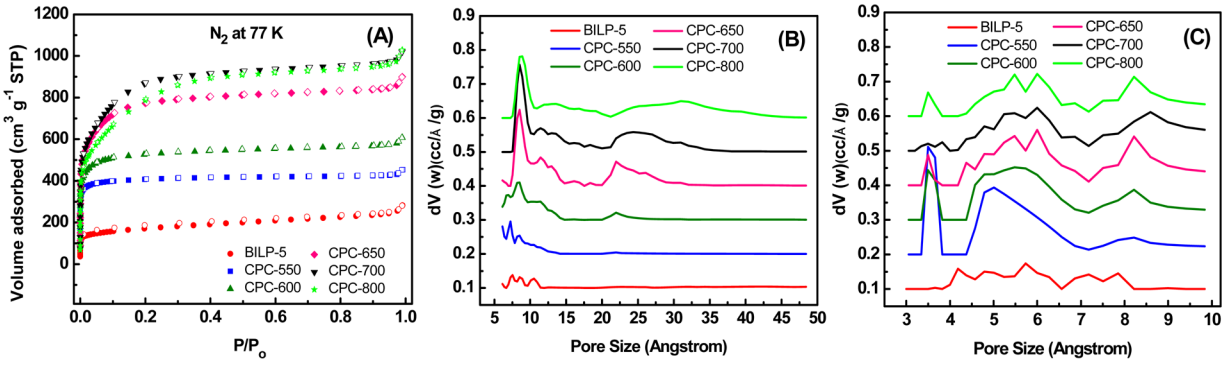

Figure 2. Nitrogen isotherms at 77 K (A) and pore size distribution from QSDFT using N_2 at 77 K (B) and from NLDFT using CO_2 at 273 K (C). (All PSD curves are offset vertically in steps of 0.1 for clarity purposes.)

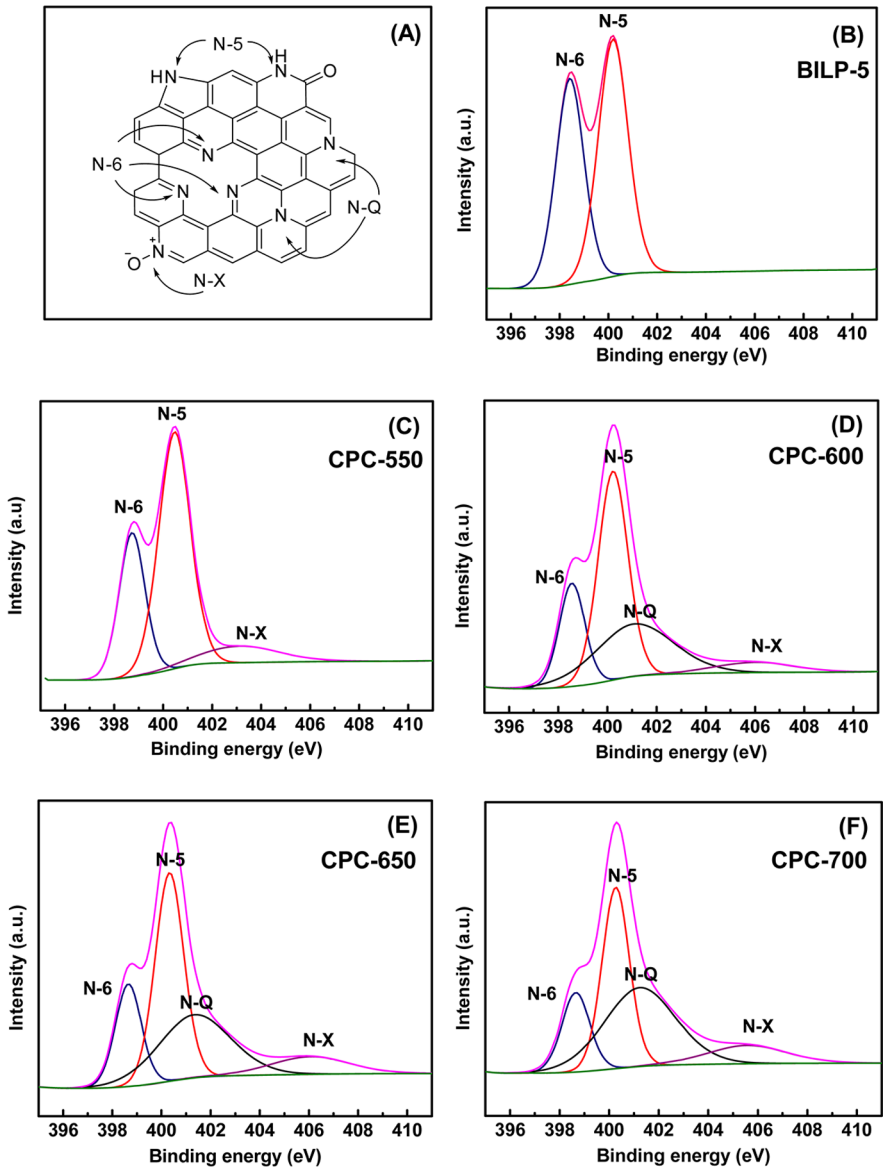

Figure 3. Schematic representation for possible nitrogen functionalities of CPCs (A) and deconvoluted N 1s spectra of BILP-5 (B), CPC-550 (C), CPC-600 (D), CPC-650 (E), and CPC-700 (F).

variety of pore size distributions from purely fine micropores to a hierarchy of micro- and narrow mesopores (2−4 nm).

The specific BET surface areas from nitrogen isotherms were calculated with respect to the consistency criteria for microporous materials as discussed in the Experimental Section and summarized in Table 1. Pore volumes were also determined from nitrogen and CO_2 adsorption isotherms using the NLDFT method. Generally, the surface area and pore volume

DOI: 10.1021/cm504435m
Chem. Mater. XXXX, XXX, XXX−XXX

Table 2. Gas Uptakes, Isosteric Heats of Adsorption, and Selectivity (CO_2/N_2 and CO_2/CH_4) for BILP-5 and CPCs[a]

	CO_2					CH_4				
	0.15 bar	1.0 bar				1.0 bar			selectivity	
sample	298 K	273 K	298 K	313 K	Q_{st}	273 K	298 K	Q_{st}	CO_2/N_2	CO_2/CH_4
BILP-5	25 (0.6)	128 (2.9)	87 (2.0)	53 (1.2)	28.5	15 (0.9)	10 (0.5)	14.6	95 (36)	10 (6)
CPC-550	94 (2.1)	367 (8.3)	256 (5.8)	189 (4.3)	35.3	43 (2.7)	27 (1.7)	21.0	65 (59)	13 (12)
CPC-600	59 (1.3)	331 (7.5)	207 (4.7)	147 (3.3)	30.8	37 (2.3)	24 (1.5)	18.5	48 (26)	10 (6)
CPC-650	40 (0.9)	297 (6.8)	176 (4.0)	117 (2.7)	24.4	35 (2.2)	21 (1.3)	19.5	24 (17)	6 (5)
CPC-700	30 (0.7)	257 (5.9)	147 (3.3)	102 (2.3)	24.2	34 (2.1)	22 (1.4)	16.2	16 (12)	4 (3)
CPC-800	31 (0.7)	236 (5.4)	137 (3.1)	88 (2.0)	27.9	32 (2.0)	20 (1.2)	18.5	19 (15)	5 (4)

[a]Gas uptake in mg g^{-1} (mmol g^{-1}), isosteric heats of adsorption (Q_{st}) in kJ mol^{-1}, and selectivity in mol mol^{-1} at 273 K (298 K).

increase with activation temperature until 700 °C and after that decrease due to over activation.[52] The specific surface area and pore volume increase significantly from 626 m^2 g^{-1} (BILP-5) to 3241 m^2 g^{-1} (CPC-700) and from 0.39 cm^3 g^{-1} (BILP-5) to 1.51 cm^3 g^{-1} (CPC-700), respectively (Table 1). The lower surface area and pore volume obtained for CPC-800 are probably related to the destruction of pore structures formed at previous steps. Porous structure development during the activation process takes place through chemical reactions between KOH and the carbon framework ($6KOH + C = 2K + 3H_2 + 2K_2CO_3$). As a result, the yield of chemically activated carbons is notably lower than porous carbons obtained by direct pyrolysis. In general the yield of activated carbons decreases by increasing the activation parameters (temperature and activator to precursor ratio). The yield of CPCs decreases from 47% to 13% by increasing the activation temperature from 550 to 800 °C implying more carbon was eliminated during the activation process (Table 1). It was also suggested that at higher activation temperatures, the products of K_2CO_3 decomposition (CO_2 and K_2O) further react with carbon and contribute more to pore formation either through gasification or lattice expansion with metallic potassium.[22] In fact, two activation pathways can be recognized for porosity formation: Low temperature activation (or low KOH/precursor) leads to initiation of pore formation followed by deepening of pores while high temperature activation results in widening of the pores generated during previous steps of activation. Depth activation contributes more micropores while width activation adds some mesopores to the system since the total micropores volume is not decreasing.[50]

It is worth mentioning that the presence of initial microprosity in BILP-5 is not necessary for micropores formation in activated carbons. According to the aforementioned mechanism, KOH activation is well-known for introducing micropores to even linear polymers such as polypyrrole[36] and polyaniline[53] or nonporous biomasses.[43] In all cases carbonization of precursor occurs through simultaneous decomposition and rearrangement of structure as temperature increases. However, considering the fact that decomposition of BILP-5 and dehydration of KOH both take place at 400 °C, that portion of initial micropores which has not completely collapsed might accelerate formation of a new micropore. Moreover, gradual increase of temperature adds mesopores to the system while the micropore volume is still increasing. A similar phenomenon was reported by Kuhn et al.[54] where simultaneous polymerization/carbonization was performed by heat treatment of nitrile monomer and zinc chloride mixture. Also it is reported that retaining some of the initial porosity during heat treatment of a sulfur rich polymer helps to further develop porous structure of the final S-doped carbon by elevating the temperature.[55]

Micropore volumes of activated carbons were calculated by two methods: *t*-plot and corresponding cumulative pore volume of pore size distribution using the DFT method. Since the *t*-plot method uses a relative pressure range of 0.2−0.4 to calculate the micropore volume, the values might deviate from the real value especially for mesoporous CPCs (2−4 nm) prepared at high temperatures. As a result, the values obtained by the DFT method would be more reliable. The ratio of $V_{Mic,DFT}/V_{Tot,DFT}$ can be considered as a degree of microporosity in CPCs and BILP-5. As shown in Table 1, the fraction of micropores can reach up to 97% of the total porosity for CPC-550 and decreases at elevated temperatures but still dominants for all CPCs. It has been reported for many carbon-based sorbents that the portion of micropores which are smaller than 0.7 nm (ultramicropores) has more pronounced effect on gas adsorption properties at ambient pressure compared to wider micropores or total pore volume.[56−58] As a result, the volume of ultramicropores was also calculated by CO_2 adsorption isotherms at 273 K. Interestingly, the amount of ultramicropores drops with increasing the activation temperature at the expense of converting some of ultramicropores to supermicropores (0.7−2 nm) or narrow mesopores (2−4 nm).

X-ray photoelectron spectroscopy (XPS) study not only confirms the successful doping of nitrogen into the frameworks of CPCs but also reveals important information about evolution of nitrogen functional groups during CPCs formation. Thus, the N 1s core level spectra of BILP-5 and all CPCs are presented in Figure 3 after peak fitting and deconvolution. The activated carbon prepared at 800 °C retains only 1 wt % of nitrogen, and unlike other specimens, its N 1s spectrum cannot be deconvoluted due to the high noise/signal ratio. As presented in Figure 3A, nitrogen atoms can be found within four different environments in CPCs: pyridinic (N-6, 398.6 eV), pyrrolic/pyridonic (N-5, 400.3 eV), quaternary (N-Q, 401.3 eV), and pyridine-N-oxide (N-X, 403.1−406.1 eV). As expected from its molecular structure, BILP-5 exhibits two peaks at 398.4 and 400.1 eV. The former is assigned to nonprotonated pyridinic whereas the latter is attributed to protonated pyrrolic nitrogen atoms both located primarily in the imidazole ring.[59] The derived CPCs contain new nitrogen species indicating chemical transformation of BILP-5 into N-rich carbons. For BILP-5 activated at 550 °C another peak around 403.1 eV appears which can be attributed to N-oxides of pyridine-N. This may result from partial oxidation of pyridinic nitrogen during activation or exposure to ambient air after activation. For CPCs prepared at 600, 650, and 700 °C a new peak located at 401.2 eV can be clearly distinguished apart from

DOI: 10.1021/cm504435m
Chem. Mater. XXXX, XXX, XXX−XXX

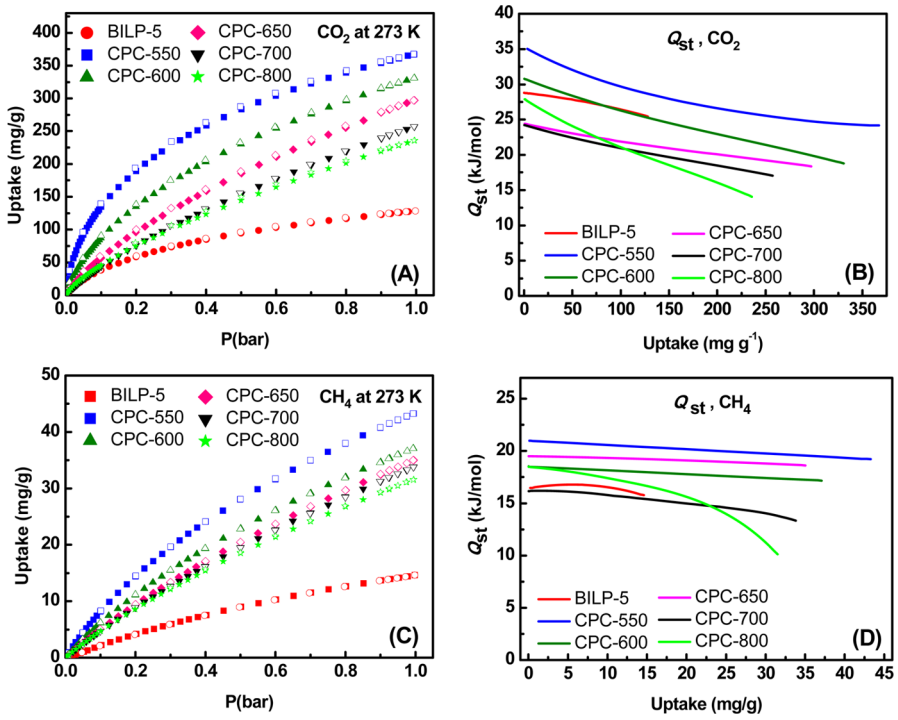

Figure 4. Gas uptake isotherms of CO_2 (A) and CH_4 (B) at 273 K and 1.0 bar and isosteric heat of adsorption of CO_2 (C) and CH_4 (D) for BILP-5 and all CPCs.

three peaks observed in CPC-550 (N-5, N-6, and N-X). The fourth peak corresponds to the most stable nitrogen form under the current activation conditions often termed quaternary or graphitic nitrogen (N-Q). It is worth mentioning that pyrrolic nitrogen might be accompanied by another type of nitrogen named pyridonic (Figure 3A). Since both pyrrolic and pyridonic takes place at same binding energy, they are not distinguishable by XPS. However, taking into consideration the oxidizing environment, temperature of activation, and presence of imidazole ring in BILP-5, it is likely to have a hybrid of both pyrrolic and pyridonic (N-5) in the prepared CPCs.

3.3. Low Pressure Gas Storage Studies. As stated above, nitrogen doped porous carbons are excellent candidates for CO_2 adsorption.[37,52,60,61] Therefore, the CO_2 capture performance of CPCs was investigated at 273, 298, and 313 K at ambient pressure as well as at 298 K/0.15 bar (CO_2 partial pressure in flue gas) as summarized in Table 2. CO_2 adsorption isotherms at different temperatures are also shown in Figure 4A and Supporting Information Figure S7A,B. Knowing that increasing the activation temperature can dramatically change the textural and chemical properties of CPCs, we investigated the effect of these parameters on CO_2 capture. It was observed that the CO_2 adsorption capacity of CPCs decreases as the activation temperature increases. Very interestingly, at 1.0 bar CPC-550 exhibits the highest CO_2 uptake (367 mg g^{-1}, 8.3 mmol g^{-1}) and (256 mg g^{-1}, 5.8 mmol g^{-1}) at 273 and 298 K, respectively. Furthermore, CPC-550 displays a high uptake of 94 mg g^{-1} (2.1 mmol g^{-1}) at 0.15 bar/298 K. To the best of our knowledge, the obtained values for CO_2 capture capacity especially at room temperature are among the highest uptakes reported to date for different types of porous carbons (Supporting Information Table S2). However, the uptake of CO_2 at 273 K/1 bar is lower than chemically activated petroleum pitch carbon (380 mg g^{-1}, 8.6 mmol g^{-1})[20] and physically activated polyacrylonitrile (507 mg g^{-1}, 11.5 mmol g^{-1}).[21] It has been well documented that microporosity plays a key role in CO_2 adsorption of various activated carbons. However, for the current CPCs, high microporous surface area, pore volume, and apparent surface area obtained for materials prepared at high activation temperatures led to a drop in CO_2 adsorption. Our observation is consistent with recent studies on a series of activated carbons that showed enhanced CO_2 uptake for samples having micropores below 0.7 nm.[53,62,63] Given the kinetic size of CO_2 (3.3 Å), CO_2 adsorption inside these pores takes place by micropore filling instead of layer by layer adsorption. According to Table 2, the CO_2 uptake has a good correlation with the volume of ultramicropores as well as the nitrogen-doping level of CPCs.

To investigate CPCs/CO_2 surface interactions, isosteric heats of adsorption (Q_{st}) were calculated by the virial method using CO_2 adsorption isotherms collected at 273 and 298 K.[64] The Q_{st} values as a function of CO_2 loading increase with nitrogen content. These values range between 24 and 35.3 kJ mol^{-1} and are comparable with those of N-doped polypyrrole-based porous carbon (19−32 kJ mol^{-1}),[43] spherical nitrogen-containing microporous carbon (25−31 kJ mol^{-1}),[46] and polyaniline-based porous carbon (21−35 kJ mol^{-1}).[53] The relatively high Q_{st} value for CPC-550 at low coverage indicates a very favorable interaction between CO_2 molecules and the chemically heterogeneous surface of the ultrafine pores. The binding affinity of CO_2 drops at higher coverage as the favorable binding sites become less accessible. These moderate heats of adsorption of CPCs provide not only a good affinity for CO_2 capture but also a facile adsorbent regeneration without heating which is vital for large scale CCS processes. To find out the mechanisms of CO_2 adsorption on the surface of CPCs both textural properties and surface chemistry should be taken into account. Three distinct regions can be distinguished in CO_2 adsorption isotherms of CPCs (Figure 4A): Low pressure (<0.2 bar) with a sharp increase in uptake,

DOI: 10.1021/cm504435m
Chem. Mater. XXXX, XXX, XXX−XXX

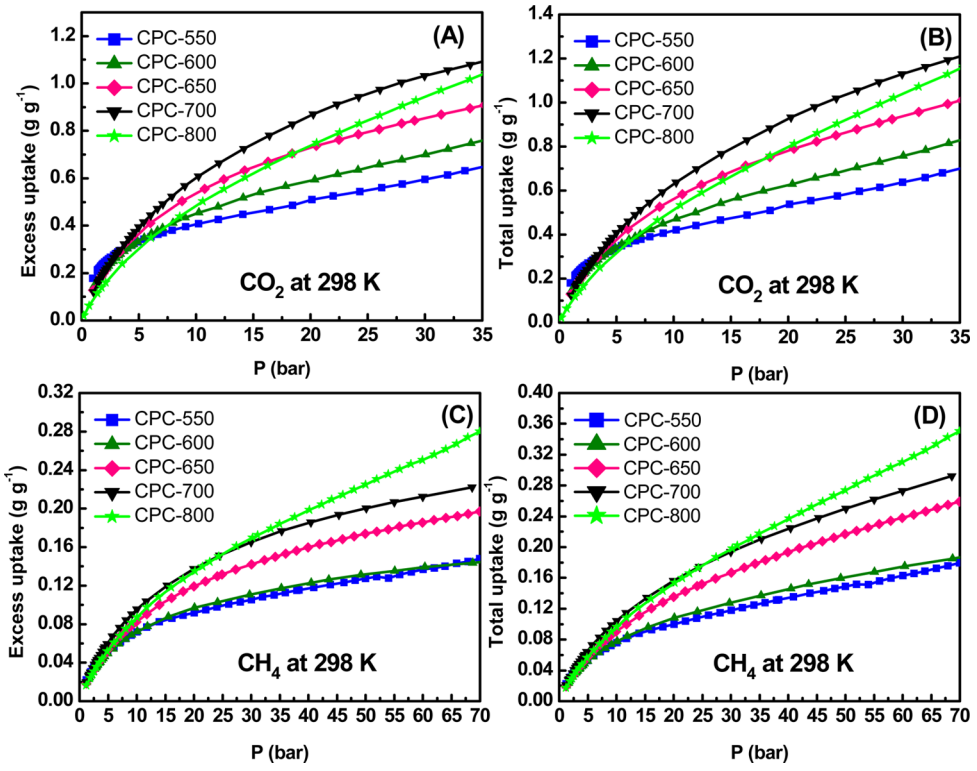

Figure 5. CO_2 high pressure excess (A) and total (B) adsorption isotherms and CH_4 excess (C) and total (D) adsorption isotherms at 298 K.

intermediate pressure (0.2−0.8), and high pressure up to 1.0 bar. As we mentioned above, CO_2 ultramicropore volume filling and interaction with nitrogen functionalities is the common adsorption mechanism in the first stage of CO_2 capture. Adsorption in the intermediate pressure range most likely takes place by filling larger micropores through layer by layer adsorption. The final step involves free volume filling by CO_2 as the pressure reaches 1.0 bar. It can be clearly seen that, as the activation temperature increases, the low pressure region shrinks and changes the overall shape of the CO_2 isotherms to a more steady increase with pressure. Notably, all isotherms are far from saturation at 1.0 bar indicating that all CPCs would accommodate more CO_2 upon applying higher pressure.

Methane uptake by CPCs was also investigated to study CO_2/CH_4 separation at low pressure and methane storage at high pressure. As summarized in Table 2 and shown in Figure 4C, activation processes resulted in methane uptake improvement for all CPCs with respect to BILP-5. The general trend of CH_4 adsorption at 1.0 bar is similar to that observed for CO_2 adsorption isotherms; CPC-550 exhibits the best methane uptake among all CPCs storing 2.7 mmol g^{-1} and 1.7 mmol g^{-1} at 273 and 298 K, respectively. These values are comparable to KOH activated carbons derived from PAF-1 (2.4 mmol g^{-1} at 273 K and 1.0 bar)[32] and the poly(vinylidene chloride)-based carbon (1.8 mmol g^{-1} at 298 K and 1 bar).[65] Therefore, at atmospheric pressure the surface area of CPCs has minimum contribution to methane uptake. Unlike CO_2, CH_4 has no quadropole moments and much lower polarizability which limit its interaction with the Lewis basic nitrogen functionalities of CPCs.[66] A simulation study on porous carbon using Grand Canonical Ensemble has shown that the optimum pore diameter for adsorption of two layers of methane should be about 0.8 nm.[67] As a result, the very high methane sorption capacity of CPC-550 can be ascribed to its higher ultramicropores volume. The Q_{st} for methane was calculated to be in a range of 16.2 to 21.0 kJ mol^{-1}. The highest was observed for CPC-550 and then dropped with higher activation temperatures up to 800 °C when the collapse of large pores reestablishes the formation of narrower pores relevant to favorable CH_4 interactions.

3.4. High Pressure Gas Storage Studies. Motivated by the high uptake of CO_2 and CH_4 at ambient pressure, we explored the storage capacity of CPCs at high pressure settings. The CO_2 excess and total adsorption isotherms are depicted in Figure 5A,B, respectively. These results indicate that, unlike low pressure uptake which is mostly governed by ultramicropores, large micropores and narrow mesopores are the predominant attributes for attaining high storage capacities at elevated pressure. Our findings are in a good agreement with a sorption study on a series of mesophase pitch derived porous carbons reported recently by Silvestre-Albero et al.[68] More specifically, they discovered that while narrow micropores have the major contribution to atmospheric CO_2 uptake, total micropore and small mesopores (2−3 nm) volumes play a key role at high pressure (up to 45 bar) uptake. Similarly, Gogotsi et al.[56] analyzed a series of activated carbons and concluded when the pressure is in the range of 1 to 10 bar, the volume of ultramicropores is the major contributor to high CO_2 uptake at 298 K. In contrast, at a pressure higher than 10 bar the uptake is mainly controlled by total pore volume of micro- and mesopores as well as the apparent surface area. A similar study on a series of porous carbons indicated that high pressure (>20 bar) CO_2 adsorption increases linearly with BET surface area, pore volume, and average pore size.[69] The highest total CO_2 uptake was recorded for CPC-700 (25.7 mmol g^{-1} at 30 bar and 298 K). This value exceeds the CO_2 adoption capacity of graphene oxide derived carbons which show similar pore volume but lower surface area.[69] This amount is also

DOI: 10.1021/cm504435m
Chem. Mater. XXXX, XXX, XXX−XXX

comparable to those of commercialized activated carbons, MAXSORB, having similar textural properties.[14,70,71] CPC-700 is outperformed by MOF-5 derived carbons due to their exceptionally high pore volume (up to 5.53 $cm^3\ g^{-1}$) and hierarchy of micro-, meso-, and macropores.[29] A petroleum pitch derived carbon, VR5-4:1, also shows superior CO_2 adsorption capacity under similar conditions owing to its higher percentage of large micropores/narrow mesopores.[68] In addition to high CO_2 uptake, the working capacity of an adsorbent is of similar significance. Table 3 lists the working capacity of CPCs at 298 K defined as the difference between total adsorption values at 30 and 1.0 bar. Not surprisingly, CPC-700 which has the highest uptake at high pressure and low uptake at 1.0 bar shows the best working capacity of ~23 mmol g^{-1}. This value is very comparable to the working capacity of the recently studied MOF-5 derived carbon (24.3 mmol g^{-1})[29] as well as most of the commercially available activated carbons including MAXSORB (21.2−24.5 mmol g^{-1}).[14,71,72]

Table 3. CH_4 and CO_2 High Pressure Uptake Characteristics of CPCs at 298 K

	CH_4 (65 bar and 298 K)			CO_2 (30 bar and 298 K)		
CPCs	excess, g g^{-1}	total, g g^{-1}	WC,[a] g g^{-1}	excess, g g^{-1}	total, g g^{-1}	WC,[a] g g^{-1}
CPC-550	0.142	0.171	0.118	0.599	0.648	0.462
CPC-600	0.143	0.182	0.130	0.705	0.763	0.618
CPC-650	0.191	0.249	0.192	0.855	0.939	0.807
CPC-700	0.218	0.284	0.219	1.033	1.131	1.007
CPC-800	0.265	0.330	0.273	0.944	1.040	0.953

[a]The working capacity is defined as the difference in total uptake between 65 to 5 bar for CH_4 and 30 to 1.0 bar for CO_2.

To see whether CPCs meet the new DOE target for methane (0.5 g/g), isotherms of CH_4 up to 65 bar at 298 K were collected. The results depicted in Figure 5C,D and summarized in Table 3 indicate that CPC-800 has the highest total storage ability of 20.5 mmol g^{-1} at 65 bar. For methane storage, it has been shown that adsorption on porous carbons at room temperature and high pressures (<30 bar) is governed by total micropore volume.[72] The improved performance of CPC-800 over CPC-700 (at P > 30 bar), despite its lower surface area, can be related to the presence of hierarchy of meso-/micropores in this sample. The storage capacity of CPC-800 reaches 66% of the new DOE gravimetric target and is comparable to similar activated carbons derived from a variety of precursors.[32,65] The deliverable methane capacity which is defined as the difference between storage and discharge pressures of 65 and 5 bar, respectively, reaches a high value for CPC-800 (0.273 g g^{-1}) due to its low uptake at low pressures and high uptake at high pressures which makes it promising for practical applications.

3. 5. Selective CO_2 Uptake Studies. In addition to their remarkably high CO_2 uptake, CPCs should exhibit facile regenerability and high selectivity for CO_2 over N_2 and CH_4 to be useful under practical conditions. To evaluate recyclability, we have selected CPC-600 and tested it by six continuous CO_2 adsorption/desorption cycles under ambient condition. As shown in Supporting Information Figure S8, CPC-600 maintains its initial CO_2 uptake capacity after six cycles, which confirms excellent recyclability of the sample. To evaluate the merit of CPCs for CO_2/N_2 and CO_2/CH_4 separation, single component adsorption isotherms of CO_2, CH_4, and N_2 were collected at 273 K/298 K and 1.0 bar for all CPCs. Utilizing these isotherms and applying Henry's law constant to their low pressure region, the initial slope ratios for all gases were calculated as summarized in Table 2 and Supporting Information Figures S9−12. Results in Table 2 show that the selectivity values of CPCs generally decrease as the activation temperature increases. It is worth mentioning that CPC-550 exhibits comparable selectivity values to BILP-5. However, the general drop in CPCs selectivity is driven by the activation process that leads to nitrogen loss, increase in surface area, and pores enlargement. The larger pores and low nitrogen content reduce CO_2 binding affinity and provide better access for N_2 and CH_4 molecules. For CPC-800, the selectivity values of CO_2 over both N_2 and CH_4 are higher than those of CPC-700 because the former has narrower pores due to partial structure collapse that favors CO_2 uptake. The optimal CO_2/N_2 selectivity value of CPC-550 at ambient temperature (59) is significantly higher than those of recently reported activated carbons such as (benzoxazine-*co*-resol)-based porous carbons (27.8),[73] N-doped microporous carbons with extra cation framework (33),[61] nitrogen doped hollow carbon nanospheres (29),[74] fungi-based carbons (18.5),[75] polypyrrole-graphene based carbons (34),[76] imine-linked derived porous carbons (12.5),[60] and algae derived carbons (10).[77]

4. CONCLUSION

In conclusion, chemical activation of benzimidazole-linked polymers with KOH followed by thermolysis afforded a series of highly porous and N-doped activated carbons with a wide range of textural properties relevant to gas storage and separation. The unique combination of high nitrogen content and ultramicroporosity in one of the prepared carbons, CPC-550, enabled high CO_2 uptake at 298 K and 1.0 bar (5.8 mmol g^{-1}). The porosity of CPCs increased significantly with activation temperature until 800 °C at which pore collapse seemed to take place. The improved textural properties (surface area and pore volume) led to very high CO_2 and CH_4 uptakes and working capacities at high pressure. In contrast, the enhanced textural properties hamper selective CO_2 separation from N_2 and CH_4 gas mixtures. For practical application of CPCs in CO_2 capture and separation, however, challenges such as reducing the cost and scalability of precursors should be addressed.

■ ASSOCIATED CONTENT

Ⓢ Supporting Information

Porosity and gas uptake studies. This material is available free of charge via the Internet at http://pubs.acs.org.

■ AUTHOR INFORMATION

Corresponding Author

*E-mail: helkaderi@vcu.edu. Fax: +1 804 828 8599. Tel: +1 804 828 7505.

Present Address

[†](S.A.) Department of Chemistry, Faculty of Science, Tafila Technical University, Tafila, 66110, P.O. Box 179, Jordan.

Funding

Research was supported by the U.S. Department of Energy, Office of Basic Energy Sciences, Division of Materials Sciences and Engineering under Award No. DE-SC0002576 and the VCU Presidential Research Initiative program.

DOI: 10.1021/cm504435m
Chem. Mater. XXXX, XXX, XXX−XXX

Notes

The authors declare no competing financial interest.

■ ACKNOWLEDGMENTS

S.A. thanks Tafila Technical University for a fellowship.

■ REFERENCES

(1) D'Alessandro, D. M.; Smit, B.; Long, J. R. *Angew. Chem., Int. Ed.* **2010**, *49*, 6058.
(2) Xia, Y.; Mokaya, R.; Walker, G. S.; Zhu, Y. *Adv. Eng. Mater.* **2011**, *1*, 678.
(3) Wang, C.; Luo, H.; Jiang, D.-e.; Li, H.; Dai, S. *Angew. Chem., Int. Ed.* **2010**, *49*, 5978.
(4) Su, F.; Lu, C. *Energy Environ. Sci.* **2012**, *5*, 9021.
(5) Akhtar, F.; Liu, Q.; Hedin, N.; Bergstrom, L. *Energy Environ. Sci.* **2012**, *5*, 7664.
(6) Nugent, P.; Belmabkhout, Y.; Burd, S. D.; Cairns, A. J.; Luebke, R.; Forrest, K.; Pham, T.; Ma, S.; Space, B.; Wojtas, L.; Eddaoudi, M.; Zaworotko, M. J. *Nature* **2013**, *495*, 80.
(7) Millward, A. R.; Yaghi, O. M. *J. Am. Chem. Soc.* **2005**, *127*, 17998.
(8) Ben, T.; Ren, H.; Ma, S.; Cao, D.; Lan, J.; Jing, X.; Wang, W.; Xu, J.; Deng, F.; Simmons, J. M.; Qiu, S.; Zhu, G. *Angew. Chem., Int. Ed.* **2009**, *48*, 9457.
(9) Dawson, R.; Stockel, E.; Holst, J. R.; Adams, D. J.; Cooper, A. I. *Energy Environ. Sci.* **2011**, *4*, 4239.
(10) Cui, S.; Cheng, W.; Shen, X.; Fan, M.; Russell, A.; Wu, Z.; Yi, X. *Energy Environ. Sci.* **2011**, *4*, 2070.
(11) Drese, J. H.; Choi, S.; Lively, R. P.; Koros, W. J.; Fauth, D. J.; Gray, M. L.; Jones, C. W. *Adv. Funct. Mater.* **2009**, *19*, 3821.
(12) Siriwardane, R. V.; Shen, M.-S.; Fisher, E. P.; Poston, J. A. *Energy Fuels* **2001**, *15*, 279.
(13) Drage, T. C.; Blackman, J. M.; Pevida, C.; Snape, C. E. *Energy Fuels* **2009**, *23*, 2790.
(14) Himeno, S.; Komatsu, T.; Fujita, S. *J. Chem. Eng. Data* **2005**, *50*, 369.
(15) Yazaydın, A. Ö.; Snurr, R. Q.; Park, T.-H.; Koh, K.; Liu, J.; LeVan, M. D.; Benin, A. I.; Jakubczak, P.; Lanuza, M.; Galloway, D. B.; Low, J. J.; Willis, R. R. *J. Am. Chem. Soc.* **2009**, *131*, 18198.
(16) Furukawa, H.; Ko, N.; Go, Y. B.; Aratani, N.; Choi, S. B.; Choi, E.; Yazaydin, A. Ö.; Snurr, R. Q.; O'Keeffe, M.; Kim, J.; Yaghi, O. M. *Science* **2010**, *329*, 424.
(17) White, R. J.; Budarin, V.; Luque, R.; Clark, J. H.; Macquarrie, D. J. *Chem. Soc. Rev.* **2009**, *38*, 3401.
(18) White, R. J.; Antonietti, M.; Titirici, M.-M. *J. Mater. Chem.* **2009**, *19*, 8645.
(19) Paraknowitsch, J. P.; Thomas, A. *Energy Environ. Sci.* **2013**, *6*, 2839.
(20) Wahby, A.; Ramos-Fernández, J. M.; Martínez-Escandell, M.; Sepúlveda-Escribano, A.; Silvestre-Albero, J.; Rodríguez-Reinoso, F. *ChemSusChem* **2010**, *3*, 974.
(21) Nandi, M.; Okada, K.; Dutta, A.; Bhaumik, A.; Maruyama, J.; Derks, D.; Uyama, H. *Chem. Commun.* **2012**, *48*, 10283.
(22) Wang, J.; Kaskel, S. *J. Mater. Chem.* **2012**, *22*, 23710.
(23) Rodríguez-Reinoso, F.; Molina-Sabio, M.; González, M. T. *Carbon* **1995**, *33*, 15.
(24) Jiang, H.-L.; Liu, B.; Lan, Y.-Q.; Kuratani, K.; Akita, T.; Shioyama, H.; Zong, F.; Xu, Q. *J. Am. Chem. Soc.* **2011**, *133*, 11854.
(25) Sevilla, M.; Fuertes, A. B. *J. Colloid Interface Sci.* **2012**, *366*, 147.
(26) Ma, Z.; Kyotani, T.; Liu, Z.; Terasaki, O.; Tomita, A. *Chem. Mater.* **2001**, *13*, 4413.
(27) Zhang, Y.; Li, B.; Williams, K.; Gao, W.-Y.; Ma, S. *Chem. Commun.* **2013**, *49*, 10269.
(28) Yang, S. J.; Kim, T.; Im, J. H.; Kim, Y. S.; Lee, K.; Jung, H.; Park, C. R. *Chem. Mater.* **2012**, *24*, 464.
(29) Srinivas, G.; Krungleviciute, V.; Guo, Z.-X.; Yildirim, T. *Energy Environ. Sci.* **2014**, *7*, 335.
(30) Lim, S.; Suh, K.; Kim, Y.; Yoon, M.; Park, H.; Dybtsev, D. N.; Kim, K. *Chem. Commun.* **2012**, *48*, 7447.
(31) Ben, T.; Li, Y.; Zhu, L.; Zhang, D.; Cao, D.; Xiang, Z.; Yao, X.; Qiu, S. *Energy Environ. Sci.* **2012**, *5*, 8370.
(32) Li, Y.; Ben, T.; Zhang, B.; Fu, Y.; Qiu, S. *Sci. Rep.* **2013**, *3*, 2420.
(33) Rabbani, M. G.; El-Kaderi, H. M. *Chem. Mater.* **2011**, *23*, 1650.
(34) Rabbani, M. G.; El-Kaderi, H. M. *Chem. Mater.* **2012**, *24*, 1511.
(35) Arab, P.; Rabbani, M. G.; Sekizkardes, A. K.; İslamoğlu, T.; El-Kaderi, H. M. *Chem. Mater.* **2014**, *26*, 1385.
(36) Sevilla, M.; Valle-Vigón, P.; Fuertes, A. B. *Adv. Funct. Mater.* **2011**, *21*, 2781.
(37) Shen, W.; Zhang, S.; He, Y.; Li, J.; Fan, W. *J. Mater. Chem.* **2011**, *21*, 14036.
(38) Bae, Y.-S.; Yazaydın, A. Ö.; Snurr, R. Q. *Langmuir* **2010**, *26*, 5475.
(39) Walton, K. S.; Snurr, R. Q. *J. Am. Chem. Soc.* **2007**, *129*, 8552.
(40) Ma, S.; Zhou, H.-C. *Chem. Commun.* **2010**, *46*, 44.
(41) Furukawa, H.; Miller, M. A.; Yaghi, O. M. *J. Mater. Chem.* **2007**, *17*, 3197.
(42) Rabbani, M. G.; Sekizkardes, A. K.; Kahveci, Z.; Reich, T. E.; Ding, R.; El-Kaderi, H. M. *Chem.—Eur. J.* **2013**, *19*, 3324.
(43) Sevilla, M.; Fuertes, A. B. *Energy Environ. Sci.* **2011**, *4*, 1765.
(44) Liu, X.; Zhou, L.; Zhao, Y.; Bian, L.; Feng, X.; Pu, Q. *ACS Appl. Mater. Interfaces* **2013**, *5*, 10280.
(45) Wickramaratne, N. P.; Jaroniec, M. *ACS Appl. Mater. Interfaces* **2013**, *5*, 1849.
(46) Liu, L.; Deng, Q.-F.; Hou, X.-X.; Yuan, Z.-Y. *J. Mater. Chem.* **2012**, *22*, 15540.
(47) Hao, G.-P.; Li, W.-C.; Qian, D.; Lu, A.-H. *Adv. Mater.* **2010**, *22*, 853.
(48) Saleh, M.; Chandra, V.; Kemp, K. C.; Kim, K. S. *Nanotechnology* **2013**, *24*, 255702.
(49) Kemp, K. C.; Chandra, V.; Saleh, M.; Kim, K. S. *Nanotechnology* **2013**, *24*, 235703.
(50) Hu, X.; Radosz, M.; Cychosz, K. A.; Thommes, M. *Environ. Sci. Technol.* **2011**, *45*, 7068.
(51) Lozano-Castelló, D.; Cazorla-Amorós, D.; Linares-Solano, A. *Carbon* **2004**, *42*, 1233.
(52) Yang, X.; Yu, M.; Zhao, Y.; Zhang, C.; Wang, X.; Jiang, J.-X. *J. Mater. Chem. A* **2014**, 2−15139.
(53) Zhang, Z.; Zhou, J.; Xing, W.; Xue, Q.; Yan, Z.; Zhuo, S.; Qiao, S. Z. *Phys. Chem. Chem. Phys.* **2013**, *15*, 2523.
(54) Kuhn, P.; Forget, A.; Su, D.; Thomas, A.; Antonietti, M. *J. Am. Chem. Soc.* **2008**, *130*, 13333.
(55) Paraknowitsch, J. P.; Thomas, A.; Schmidt, J. *Chem. Commun.* **2011**, *47*, 8283.
(56) Presser, V.; McDonough, J.; Yeon, S.-H.; Gogotsi, Y. *Energy Environ. Sci.* **2011**, *4*, 3059.
(57) Wei, H.; Deng, S.; Hu, B.; Chen, Z.; Wang, B.; Huang, J.; Yu, G. *ChemSusChem* **2012**, *5*, 2354.
(58) Sevilla, M.; Parra, J. B.; Fuertes, A. B. *ACS Appl. Mater. Interfaces* **2013**, *5*, 6360.
(59) Hua, M.-Y.; Chen, H.-C.; Tsai, R.-Y.; Lai, C.-S. *Talanta* **2011**, *85*, 631.
(60) Wang, J.; Senkovska, I.; Oschatz, M.; Lohe, M. R.; Borchardt, L.; Heerwig, A.; Liu, Q.; Kaskel, S. *J. Mater. Chem. A* **2013**, *1*, 10951.
(61) Zhao, Y.; Zhao, L.; Yao, K. X.; Yang, Y.; Zhang, Q.; Han, Y. *J. Mater. Chem.* **2012**, *22*, 19726.
(62) Pevida, C.; Drage, T. C.; Snape, C. E. *Carbon* **2008**, *46*, 1464.
(63) Martín, C. F.; Plaza, M. G.; Pis, J. J.; Rubiera, F.; Pevida, C.; Centeno, T. A. *Sep. Purif. Technol.* **2010**, *74*, 225.
(64) Czepirski, L.; JagieŁŁo, J. *Chem. Eng. Sci.* **1989**, *44*, 797.
(65) Cai, J.; Qi, J.; Yang, C.; Zhao, X. *ACS Appl. Mater. Interfaces* **2014**, *6*, 3703.
(66) Herm, Z. R.; Krishna, R.; Long, J. R. *Microporous Mesoporous Mater.* **2012**, *151*, 481.
(67) Mosher, K.; He, J.; Liu, Y.; Rupp, E.; Wilcox, J. *Int. J. Coal Geol.* **2013**, *109−110*, 36.
(68) Casco, M. E.; Martínez-Escandell, M.; Silvestre-Albero, J.; Rodríguez-Reinoso, F. *Carbon* **2014**, *67*, 230.

DOI: 10.1021/cm504435m
Chem. Mater. XXXX, XXX, XXX−XXX

(69) Srinivas, G.; Burress, J.; Yildirim, T. *Energy Environ. Sci.* **2012**, *5*, 6453.
(70) Marco-Lozar, J. P.; Juan-Juan, J.; Suárez-García, F.; Cazorla-Amorós, D.; Linares-Solano, A. *Int. J. Hydrogen Energy* **2012**, *37*, 2370.
(71) Saha, B. B.; Jribi, S.; Koyama, S.; El-Sharkawy, I. I. *J. Chem. Eng. Data* **2011**, *56*, 1974.
(72) Marco-Lozar, J. P.; Kunowsky, M.; Suarez-Garcia, F.; Carruthers, J. D.; Linares-Solano, A. *Energy Environ. Sci.* **2012**, *5*, 9833.
(73) Hao, G.-P.; Li, W.-C.; Qian, D.; Wang, G.-H.; Zhang, W.-P.; Zhang, T.; Wang, A.-Q.; Schüth, F.; Bongard, H.-J.; Lu, A.-H. *J. Am. Chem. Soc.* **2011**, *133*, 11378.
(74) Zhou, L.; Shao, Y.; Liu, J.; Ye, Z.; Zhang, H.; Ma, J.; Jia, Y.; Gao, W.; Li, Y. *ACS Appl. Mater. Interfaces* **2014**, *6*, 7275.
(75) Xing, W.; Liu, C.; Zhou, Z.; Zhang, L.; Zhou, J.; Zhuo, S.; Yan, Z.; Gao, H.; Wang, G.; Qiao, S. Z. *Energy Environ. Sci.* **2012**, *5*, 7323.
(76) Chandra, V.; Yu, S. U.; Kim, S. H.; Yoon, Y. S.; Kim, D. Y.; Kwon, A. H.; Meyyappan, M.; Kim, K. S. *Chem. Commun.* **2012**, *48*, 735.
(77) Sevilla, M.; Falco, C.; Titirici, M.-M.; Fuertes, A. B. *RSC Adv.* **2012**, *2*, 12792.

DOI: 10.1021/cm504435m
Chem. Mater. XXXX, XXX, XXX−XXX